

Preliminary evaluation of the effect of electro-coalescence with conducting sphere approximation on the formation of warm cumulus clouds using SCALE-SDM version 0.2.5-2.3.0

5 Ruyi Zhang¹, Limin Zhou^{1,2}, Shin-ichiro Shima^{3,4}, Huawei Yang¹

¹Key Laboratory of Geographic Information Science, Ministry of Education, East China Normal University, Shanghai, 200241, China

²Key Laboratory of Numerical Modeling for Atmospheric Science and Geophysical Fluid Dynamics, Institute of Atmospheric Physics, CAS, Beijing, 100029, China

10 ³Graduate School of Simulation Studies, University of Hyogo, Kobe, 6512103, Japan

⁴RIKEN Center for Computational Science, Kobe, 6500047, Japan

Correspondence to: Limin Zhou(lmzhou@geo.ecnu.edu.cn)

Abstract. The phenomenon of electric fields applied to droplets inducing droplet coalescence is called
15 the electro-coalescence effect. An analytic expression for electro-coalescence with the accurate electrostatic force for a pair of droplets with opposite sign charges is established by treating the droplets as conducting spheres (CS). To investigate this effect, we applied a weak electric field to a cumulus cloud using a cloud model that employs the super-droplet method, a probabilistic particle-based microphysics method. This study employs a two-dimensional large eddy simulation in a flow-coupled model to
20 examine aerosol microphysics (such as collision-coalescence enhancement, velocity fluctuations, and supersaturation fluctuations) in warm cumulus clouds without relying on subgrid dynamics. In the simulation, we assume that droplets carry opposite sign charges and are well mixed within the cloud. The charge is not treated as an individual particle attribute. To assess fluctuation effects, we conducted 50 simulations with varying pseudo-random number sequences for each electro-coalescence treatment. The
25 results show that with CS treatment, the electrostatic force contributes a larger effect on cloud evolution than previous research. With lower charge limit of the maximum charge amount on the droplet, the domain total precipitation with CS treatment for droplets with opposite signs is higher than that with the no charge setting. Compared to previous work, the multi-image-dipole treatment of CS results in higher precipitation. It is found that the electro-coalescence effect could affect rain formation even when the
30 droplet charge is at the lower charge limit. High pollution levels result in greater sensitivity to electro-coalescence. The results show that when the charges ratio between two droplets is over 100, the short-range attractive electric force due to the multi-image dipole would also significantly enhance precipitation for the cumulus. It is indicated that although the accurate treatment of the electrostatic force with CS method would require 30 % longer computation time than before, it is worthwhile to include it
35 in cloud, weather, and climate models.

1 Introduction

Clouds are considered to play a key role in climate systems, and the collision-coalescence of cloud droplets plays a key role in rain formation. Droplet coalescence is one of the main processes leading to precipitation, affecting cloud microphysics and thereby changing the global radiation budget (Pruppacher and Klett, 2010, Chapter 15; Grabowski and Wang, 2013; IPCC AR6 WG1 Ch7, 2021). Several studies have reported that the electrostatic force on charged droplets could significantly influence the droplet coalescence and droplet-aerosol coagulation in weakly electrified clouds (Rayleigh, 1879; Tinsley et al., 2001, 2006; Zhou et al., 2009; Tripathi et al., 2008; Pruppacher and Klett, 2010; Zhang et al., 2018; Guo and Xue, 2021). This electrostatic force induced effect is called electro-coalescence or electro-anti-coalescence (Tinsley, 2008) and could even explain the link between solar wind fluctuations and changes in atmospheric parameters, such as cloud cover, polar surface pressure and the effective radiation in polar regions (Kniveton et al., 2008; Lam et al., 2014; Frederick & Tinsley, 2018; Frederick et al., 2019).

In weakly electrified clouds, the accumulation of space charges on droplets is controlled by the diffusion of atmospheric ions produced by the cosmic ray flux, and the concentration is dependent on the ratio of attachment and recombination and the downward ionosphere-earth current density (J_z). When the J_z penetrates the cloud, the gradients of the electric field at the cloud boundary could generate net positively charged droplets at the upper cloud boundary and net negatively charged droplets at the lower boundary (Zhou and Tinsley, 2007; Nicoll and Harrison, 2016). The observations of Beard et al. (2004) revealed that with a J_z of $1\text{-}6 \text{ pAm}^{-2}$ in stratocumulus and altostratus clouds, a cloud droplet with the radius of $10 \mu\text{m}$ can accept approximately 100 elemental charges, which is consistent with the theoretical calculations by Zhou and Tinsley (2007). In cumulus clouds, vertical convection causes positive charge droplets from the upper boundary and negative charge droplets from the lower boundary to mix, leading to electro-coalescence. The maximum charge on the droplets is determined by the air breakdown voltage for corona discharge (Meek and Carggs, 1953) and is a quadratic function of the droplet radius (Khain et al., 2004; Andronache, 2004).

Numerous studies have focused on parameterizing the microphysics of the electro-coalescence of particles, the challenge is to approximate calculation the electrostatic force between charged droplets. In the 1970s, the collision efficiency of oppositely charged droplets evaluated with a centered Coulomb force (CB) indicated that only in strongly electrified clouds can the charge on droplets significantly affect cloud droplet coagulation (Wang et al., 1978). The trajectory simulation studies by Tinsley et al. (2001, 2006), Tripathi et al. (2006), and Zhou et al. (2009) revealed that in a weakly electrified cloud, when taking into account the image charge force, the collision rate coefficient between the charged droplets could be different. Even with droplet charges of the same sign, the collision rate coefficient could be enhanced as a function of the charge on the particles with radii ranging from $0.1 \mu\text{m}$ to $10 \mu\text{m}$ (Zhou et al., 2009). The so-called Greenfield gap, identified by Greenfield (1957), describes the reduced concentrations of particles in the 0.1 to $1 \mu\text{m}$ size range. Greenfield gap could be reduced with sufficient charging of the droplets. Simulation results showed that for particles with radii smaller than $0.1 \mu\text{m}$, when the particles obtain a large charge due to the evaporation of highly charged droplets, the collision rate coefficient is significantly decreased due to the repulsive electric force of droplets with charges of the same sign and is increased for charges of the opposite sign (Tinsley and Leddon, 2013). The updated

simulation by Zhou et al. (2009) with an exact electric force treatment with the conducting sphere (CS) method indicated that the collision efficiency is a factor of two higher in the Greenfield gap than that from the results of single image charge (IM) treatment. A few laboratory experiment results were consistent with these theoretical simulations (Ardon-Dryer et al., 2015). These findings highlight the need to represent coagulation due to droplet and aerosol charges in the cloud model. Khain et al. (2004) (hereafter Khain04) conducted a 0-dimension simulation to study the effect of seeding charged droplets on a cumulus cloud using the spectral bin cloud model with a 4-dimensional (mass and charging rate of two droplets) collision efficiency lookup table based on the static electric force between charged droplets. The results showed a significant response in the evolution of clouds due to charged droplets. Khain04 set a charging rate equal to 5 % of the maximum charge of natural droplets, which is 2.5 times larger than the values reported by Zhou et al. (2007), to study electro-coalescence impact on rain enhancement and fog elimination. Andronache (2004) and Wang et al. (2015) claimed that charged droplets significantly contribute to below cloud scavenging according to the analytical formula suggested by Davenport and Peters (1978), where the minimum amount of charge on droplets is 7 % of the maximum limit. However, only CB treatment was used in Andronache (2004) and Wang et al. (2015) simulations.

Lagrangian particle-based approaches accurate solutions for the collision-coalescence process compared to bin microphysics schemes, as they overcome the limitations imposed by the assumptions of bin schemes (Grabowski et al., 2019; Liu et al., 2023). In this study, we estimate the effect of electro-coalescence from J_z on warm cumulus clouds by an exact treatment of electric forces using the CS method, using the Super-Droplet Method (SDM), a Lagrangian particle-based cloud microphysics scheme. The lower charging rate threshold for electro-coalescence is discussed. The extreme assumption of the droplet charging scenario of opposite sign charge is investigated. The electro-anti-coalescence (Tinsley and Zhou, 2015) between charged droplets and particles could also be important for deep convection and stratus cloud evolution.

2. Description of the cloud model

In this study, we assume that the charged droplets are well-mixed in the warm cumulus cloud and focus on the electro-coalescence effect. A Lagrangian particle-based cloud model is used with the particle size resolved treatment following the SDM by Shima et al. (2009, 2020). Compared to bin microphysics schemes, SDM eliminates numerical diffusion and provides more accurate solutions for well-mixed volumes (Grabowski et al., 2019). Despite its sensitivity to super-droplet initialization and a higher variance than observed in reality (Liu et al., 2023), SDM is well-suited for this study. This section provides a description of the SDM, how we generalize the exact electric force treatment with the CS method approach for the cloud model, and the numerical simulation setup.

2.1 Definition of super-droplets

Super-droplets have been defined in detail by Shima et al. (2009, 2020). A super-droplet represents multiple droplets with the same attributes and position, and this multiplicity is denoted by the positive

integer $\xi_i(t)$, which can be different in each super-droplet and is time-dependent due to the definition of coalescence. Then, each super-droplet has its own position $x_i(t)$ and its own attributes $a_i(t)$ that characterize the $\xi_i(t)$ identical droplets represented by super-droplet i . In this study, we assume that the attributes consist of the equivalent radius and the mass in the droplet $a_i(t) = [R_i(t), M_i(t)]$. Since each real droplet takes different positions and attributes, a super-droplet is a kind of coarse-grained view of droplets both in real space and attribute space. Assume that $N_s(t)$ is the number of super-droplets in the domain at time t . Then, the super-droplets represent $N_r(t) = \sum_{i=1}^{N_s(t)} \xi_i(t)$ real droplets in total.

120

2.2 Motion of a super-droplet

The advection and sedimentation processes were described in detail by Shima et al. (2009, 2020) as follows:

$$125 \quad \frac{d(m_i v_i)}{dt} = F_i^{drg} - m_i g \hat{z} \quad (1)$$

where $m_i = (4\pi/3)R_i^3 \rho_{liq}$ is the mass of droplet i , and $\rho_{liq} = 1.0 \text{ g} \cdot \text{cm}^{-3}$ is the density of liquid water.

$F_i^{drg} = m_i g \hat{z} + d(m_i v_i)/dt$ is the drag force from moist air, g is the gravity of Earth, and \hat{z} is the unit vector in the direction of the z-axis. $-F_i^{drg}$ gives the reaction force acting on the moist air (Montero-Martínez et al., 2009). Considering that the relaxation to the terminal velocity is instantaneous, and the

130 equation of motion becomes:

$$v_i = U_i - \hat{z} v_i^\infty, \frac{dx_i}{dt} = v_i \quad (2)$$

where $U_i = U(x)$ is the ambient wind velocity of the i -th particle, v_i^∞ is the terminal velocity, which in general is a function of the attributes α_i and the state of the ambient air.

The motion of a super-droplet is the same as that of a droplet, which is described in Eq. (2), and $v_i(t)$

135 is equal to the terminal velocity.

2.3 Condensation and evaporation

The condensation/evaporation process is based on Köhler's theory, which takes into account the solution and curvature effects on the droplet's equilibrium vapour pressure (Köhler, 1936; Rogers & Yau, 1989; Pruppacher and Klett, 2010, Chapter 13). The growth equation of radius R_i is derived as follows:

$$140 \quad R_i \frac{dR_i}{dt} = \frac{(S-1) - \frac{a}{R_i} + \frac{b}{R_i^3}}{F_k + F_d} \quad (3)$$

$$F_k = \left(\frac{L}{R_v T} - 1 \right) \frac{L \rho_{liq}}{KT}, F_d = \frac{\rho_{liq} R_v T}{De_s(T)} \quad (4)$$

where S is the ambient saturation ratio; F_k represents the thermodynamic term associated with the latent heat release; F_d represents the term associated with vapour diffusion; the term a/R_i represents the

curvature effect, which expresses the increase in the saturation ratio over a droplet compared with that
 145 of a plane surface; the term b/R_i^3 represents the reduction in the vapour pressure due to the presence of
 a dissolved substance, where b depends on the mass of solute M_i dissolved in the droplet;
 $a \approx 3.3 \times 10^{-5} \text{ cm K } T^{-1}$ and $b \approx 4.3 \text{ cm}^3 i M_i m_s^{-1}$, where T is the temperature, $i \approx 2$ is the degree of
 ionic dissociation and m_s is the molecular weight of the solute. R_v is the individual gas constant for water
 vapour, K is the coefficient of thermal conductivity of air, D is the molecular diffusion coefficient, L is
 150 the latent heat of vaporization, $e_s(T)$ is the saturation vapour pressure. Note the charge-induced reduction
 in surface tension decreases the equilibrium vapor pressure (Weon & Je, 2010).

2.4 Collision-coalescence and the electric effect

In warm clouds, the collision-coalescence of two droplets to form a larger droplet is responsible for
 155 precipitation and cloud lifetime. The droplet growth due to the coalescence is controlled by the net action
 of various forces impacting the relative motion of the two droplets. The effective collision-coalescence
 of droplets can be evaluated by the collision-coalescence kernel K , which can be described as follows:

$$K = \pi E \left((R+r)^2 |v_R^\infty - v_r^\infty| \right) + K_B \quad (5)$$

where $E = E_0(R+r) + E_{es}(R, Q_R, r, q_r)$ is the collision-coalescence efficiency, and K_B is the Brownian
 160 coagulation kernel. Respectively, R represents the radius of the larger droplet, r is the radius of smaller
 droplets of given pair (R, r) . Similarly, Q_R represents the charge of larger droplets, q_r is the charge
 of smaller droplets. And v_R represents the terminal velocity of larger droplets, v_r is the terminal
 velocity of smaller droplets. In this study, we assume

$E_0(R, r)$ takes into account the effect of a small droplet/particle being swept by the stream flow around
 165 a larger droplet or bouncing on the surface by front, side or rear collection, or droplets of similar size
 collide on the downstream side and are caught (Davis, 1972; Hall, 1980; Jonas, 1972; Pruppacher and
 Klett, 2010, chapter 14). Following Seeßelberg et al. (1996) and Bott (1998), the collision efficiency of
 Davis (1972) and Jonas (1972) for small droplets and the collision efficiency of Hall (1980) for large
 droplets are adopted. We assume the coalescence efficiency is unity in this study.

170 The Brownian coagulation kernel K_B is given by Seinfeld and Pandis (2006, chapter 13) using Fuchs
 (1964) corrected factor to correct the boundary condition of absorbing particles surface. The Fuchs Form
 of Brownian coagulation coefficient is derived as follows:

$$K_B = 2\pi(D_1 + D_2)(D_{p1} + D_{p2}) \left(\frac{D_{p1} + D_{p2}}{D_{p1} + D_{p2} + 2(g_1^2 + g_2^2)^{1/2}} + \frac{8(D_1 + D_2)}{(\bar{c}_1^2 + \bar{c}_2^2)^{1/2}(D_{p1} + D_{p2})} \right)^{-1} \quad (6)$$

Where:

$$175 \quad \bar{c}_i = \left(\frac{8kT}{\pi m_i} \right)^{1/2} \quad (7)$$

$$\ell_i = \frac{8D_i}{\pi \bar{c}_i} \quad (8)$$

$$g_i = \frac{\sqrt{2}}{3D_{pi}\ell_i} \left[(D_{pi} + \ell_i)^3 - (D_{pi} + \ell_i^2)^{3/2} \right] - D_{pi} \quad (9)$$

$$D_i = \frac{kTC_c}{3\pi\mu D_{pi}} \quad (10)$$

180 ℓ_i represents particle mean free path, D_i represents Brownian diffusivity; D_{pi} represents diameters of particles, m_i is particle mass, $k = 1.381 \times 10^{-23} \text{ J K}^{-1}$ is the Boltzmann constant, μ represents the dynamic viscosity of air and C_c is a slip correction factor.

Referring to Andronache (2004), we propose a parameterization of the collision efficiency due to the electric force $E_{es}(R, Q_R, r, q_r)$ based on the work by Zhou et al. (2009) and Tinsley and Zhou (2015).

185 The induced charge on the droplet is involved in our E_{es} . Based on the trajectory model simulation, the electric force with the IM treatment (Tinsley et al., 2006) and the CS treatment (Zhou et al., 2009) can significantly contribute to the collision efficiency. For droplets with opposite sign charges, in the front and side collision ranges, the short-range attractive electric force due to the induced image charge provides additional force to balance the repulsive force. In the rear collision range, this short-range attractive force contributes to balancing the inertia. The rear collision range is relevant for droplets
190 smaller than $0.1 \mu\text{m}$, the droplets typically accept fewer than 1 elemental charge, meaning the electric force does not significantly impact the collision process. Therefore, the main electric force remains in the side and front collision range and droplets accept more than 1 elemental charge in this study.

The analytical parameterization for the collision efficiency with the electric force suggested by Davenport and Peters (1978) is used with modification to include the image charge effect of opposite
195 charged droplets in our study. Tinsley and Zhou (2015) developed same charged droplets charge effect.

$$E_{es} = \frac{4c_f}{6\pi\mu Rv} \cdot F_{es} \quad (11)$$

where c_f is the Cunningham correction factor, v is the terminal velocity of the droplet. F_{es} is the electric force between the colliding droplets.

In this study, F_{es} is calculated in four different ways, namely, CB, IM, Khain04, and CS, which are given
200 by Eqs. (13-16), respectively.

CB treatment considers only the Coulomb force between the centre points of the droplets. Then, F_{es} is given by

$$F_{es} = \frac{1}{4\pi\epsilon_0} \frac{Q_R q_r}{R_b^2} \quad (12)$$

205 Where $\epsilon_0 = 8.854 \times 10^{-12} \text{ F m}^{-1}$ is the dielectric permittivity of free space. Q_R and q_r are charge of large and small particles. R_b is the distance between the centre of two droplets.

Khain04 used the superposition method to calculate a four-dimensional (with respect to droplet size and charge) lookup table for collision efficiency, and present an approximated solution for electrostatic forces of droplet by following formula:

$$F_{es} \approx \frac{Q_R q_r}{4\pi\epsilon_0 R_b^2} + \frac{1}{4\pi\epsilon_0} \left\{ Q_R^2 \left[\frac{1}{R_b^3} - \frac{R_b}{(R_b^2 - r^2)^2} \right] + q_r^2 R \left[\frac{1}{R_b^3} - \frac{R_b}{(R_b^2 - R^2)^2} \right] \right. \\ \left. + Q_R q_r R r \left[\frac{1}{R_b^4} + \frac{1}{(R_b^2 - R^2 - r^2)^2} - \frac{1}{(R_b^2 - R^2)^2} - \frac{1}{(R_b^2 - r^2)^2} \right] \right\} \quad (13)$$

210 R and r represents the radius of larger and smaller droplet of a pair droplet. Note that in this study, we calculate collision-coalescence kernel of Khain04 method by Eq. (13) for electrostatic forces and Eq. (11) for charge effect, whereas Khain04 used a 4-dimensional lookup table for collision efficiency.

The distance parameter r_{nt} is needed to calculate F_{es} of IM and CS treatment. Based on the trajectory simulation results by Zhou et al. (2009), r_{nt} is fitted as follows:

$$215 \quad r_{nt} = \frac{r}{R} \left[1 + r_{ref} \cdot \left(\frac{R}{r/2} \right) + \frac{R}{r} \right] \quad (14)$$

where $r_{ref} = 0.01$.

When the large droplet radius is 100 times larger than the small droplet radius, the IM treatment, is accurate enough. F_{es} for IM treatment is given by:

$$F_{es} = \frac{4Cq_r^2}{(d_p/2)^2} \left[\frac{r_{nt}}{(r_{nt}^2 - 1)^2} + \frac{1}{r_{nt}^2} \cdot \left(\frac{Q_R}{q_r} - \frac{1}{r_{nt}} \right) \right] \quad (15)$$

220 where $C = 9 \times 10^9$ (in $N m^2 C^{-2}$).

If the ratio between the droplet and particle is less than 100, the electric force is treated by the CS method according to Zhou et al. (2009), which originates from Davis (1964):

$$F_{es} = 4C \cdot \left(q_r Q_R \frac{F_6}{r^2} + q_r^2 \frac{F_7}{r^2} + Q_R^2 \frac{F_5}{r^2} \right) \quad (16)$$

225 where F_5 , F_6 , and F_7 are dimensionless complex polynomial expressions given by Davis (1964) that depend only on the radii of the two droplets and their distance parameter r_{nt} .

In this study, we assume that J_z charges the droplets. Zhou and Tinsley (2012) observed that droplets with a 10 μm radius achieve 70 % of their charge in 680 seconds. However, following Andronache (2004) simplification of the complex charging process, we assume that the charge on droplets resulting from collision-coalescence reaches equilibrium instantaneously. We also consider an extreme scenario where
230 the charge polarity of two colliding droplets is always opposite. The assumption of instantaneous charging might lead to an overestimation of the electro-coalescence effect. Regarding the charge polarity, convective mixing within cumulus clouds introduces oppositely charged droplets from the cloud boundary into the cloud interior. These droplets retain their opposite charges due to the relatively long discharge timescale, significantly impacting the early stages of raindrop formation. The coalescence of
235 large rain droplets is dominated by gravity settling. Notably, Khain (2004) addressed charge differences by subtracting the charge of opposite polarity particles and adding the charge of same polarity particles after collision-coalescence.

The voltage near a charged spherical particle is described by $U = q / 4\pi\epsilon_0 r^2$ (Bleaney and Bleaney, 1993).

The air breakdown voltage: $U_b \sim 3 \times 10^6 \text{ V m}^{-1}$, determines the maximum charge that cloud droplets

240 can carry (Meek and Craggs, 1953). Consequently, the maximum charge that droplets can carry is as follows:

$$q_{\max} = 4\pi U_b \varepsilon_0 r^2 \quad (17)$$

To simulate droplets in a weak electric field, we followed Andronache (2004) and described the mean charges on the larger and smaller droplets in a pair as a function of their radii as follows:

$$245 \quad Q_R = 4\alpha AR^2, q_r = 4\alpha Ar^2 \quad (18)$$

Here $A = \pi \times U_b \times \varepsilon_0 \times 10^{-2} = 0.83 \times 10^{-6}$ is two orders of magnitude smaller than the maximum particle charge, representing weakly charge condition, and the charging rate α is an empirical parameter (α is referred to herein as the droplet charging rate) that varies between 0, which represents neutral particles, and 7, which represents highly electrified clouds associated with thunderstorms (Andronache, 2004). In our work, the α value ranges from 0.1 to 0.6, which represents a weakly electrified cloud. Compared with the maximum charge of the droplet method used by Khain04, when α ranges from 0.1 to 0.6 cm^{-2} , the charge on the droplet reaches 0.3 % up to 2 % of the maximum charge, which is 10 times to 2 times smaller than the lowest value used by Khain04 and Wang et al. (2015). The minimum limit for the droplet charge is equivalent to 1 elemental charge. This could be a reliable estimation for the accumulated charge on droplets with the downward current density (J_z) since a droplet with a radius of 10 μm can accept 255 200 elemental charges when $\alpha=0.1$, which is consistent with the stratus cloud charge distribution simulation by Zhou and Tinsley (2007, 2012).

Figure 1 displays a comparison of the collision-coalescence kernel for droplet radii of 40 μm (black lines), 20 μm (green lines), and 10 μm (red lines) across different calculation methods. The plots vary by line style to represent different analytical treatments and the inclusion or absence of static electric forces, with specific settings for the droplet charging rate shown in Fig. 1(a) and Fig. 1(b). The results indicate that the primary range for electro-coalescence is approximately 0.1 μm to 10 μm , which encompasses the Greenfield gap. When the small droplet radius is less than 0.1 μm , the collision process is controlled by Brownian motion due to an excessively small number of charges on the small droplet. Conversely, when the radius of the droplets exceeds 10 μm , the collision process is primarily governed by gravity collision. The electric force has a larger effect on the smaller droplet. The electric force treated with the CS method has a larger effect on the collision-coalescence kernel than that of the IM method and the CB method. In the range of the Greenfield gap, the collision-coalescence kernels from the analytical method fit well with those with the trajectory method result. Note that CB, Khain04 and IM method does not take into account the collision of same size droplets, for CS method, the Q^2 term provide attractive or repulsive force between same size droplets ensures collision. For the range of droplets smaller than 10 μm , when the particle radius is close to 10 μm , CB, Khain04 and IM method deviates from the trajectory result, but the result of the CS method becomes over 2 times less than that of the trajectory method, where the collision process is controlled by the interception effect. The interception effect in particle collision coalescence refers to the process where smaller particles are captured by a larger droplet's boundary layer and swept into it, even without direct contact, due to the aerodynamic airflow around the falling droplet. Although the analytical method cannot reproduce the interception effect, it can give the lower limit of estimation to the effect of the electric force effect with the conducting sphere method.

280 **2.5 Numerical setup and schemes**

Shima et al. (2009, 2020) constructed a particle-based cloud model SCALE-SDM by implementing the SDM into SCALE, which is a library of weather and climate models of the Earth and other planets (Nishizawa et al., 2015; Sato et al., 2015). Because of its efficient Monte Carlo algorithm for coalescence, the particle-base scheme SDM requires less computational cost to accurately simulate clouds and precipitation compare to bin scheme (Shima et al., 2009). This study concentrates on warm-rain microphysics. We developed a numerical simulation using the latest version of SCALE-SDM, specifically employing the SDM warm rain algorithm from Shima et al. (2009), rather than the SDM mixed-phase extension presented by Shima et al. (2020). We implemented the electro-coalescence process into SDM’s coalescence scheme as defined by Eqs. (5)-(18). The moist air fluid dynamics in this study are computed using Eqs. (71)-(81) of Shima et al. (2020). The calculations utilize SCALE’s dynamical core, which is based on fully-compressible non-hydrostatic equation. This approach is implemented on an Arakawa-C staggered grid (Arakawa and Lamb, 1977) using a finite volume method. For the initialization of the super-particle, the “uniform sampling method” is applied as in previous works (Arabas and Shima, 2013; Shima et al., 2014, 2020; Sato et al., 2017, 2018). Unterstrasser et al. (2017) found that the uniform sampling method is more efficient than the “constant multiplicity method”. Then, the multiplicity of the super-droplets becomes proportional to the initial distribution function of real particles:

$$\xi(a, x) = n(a, x, t = 0) / (N_s(0)p) \quad (19)$$

$$p(a, x) = p = \text{constant} \quad (20)$$

300 In SCALE-SDM, moist air dynamics and cloud microphysics processes are integrated separately by using the 1st-order operator splitting scheme. Δt is set as the common time step. We set Δt_{adv} , $\Delta t_{cnd/evp}$, and Δt_{coal} as the time steps for the advection and sedimentation of particles, condensation/evaporation, and collision-coalescence. We set Δt_{dyn} as the time step for the fluid dynamics of moist air, which has to fulfil the Courant-Friedrichs-Lewy (CFL) condition of acoustic waves. All these time steps are divisors of the common time step Δt . The order of calculation in the model is as follows: 1) calculate the fluid dynamics without the coupling terms from the particles to moist air, and update the moist air; 2) update the super-droplets $\{\{\zeta_i, x_i, a_i\}\}$ from t to $t + \Delta t$. 3) We integrate one cloud microphysics process one time step forward and then moves on to the next process. Processes lagging in time are calculated preferentially (for details, refer to Table 1 of Shima et al., 2020). Simultaneously, the feedback from particles to moist air comes through the coupling terms of Eqs. (75)-(79) of Shima et al. (2020), and we update the moist air from $G_{min}(t)$ to $G_{min}(t + \Delta t)$.

315 In our simulation, the domain of the simulation is two dimensional (x-z), 10 km in the horizontal and vertical directions with 50 m grid spacing, and the calculation time steps are $\Delta t = 0.4$ s, $\Delta t_{dyn} = 0.05$ s, $\Delta t_{adv} = 0.4$ s, $\Delta t_{cnd/eva} = 0.1$ s, and $\Delta t_{coal} = 0.2$ s. Initial super droplet number concentration per grid cell is 128. We employ a subgrid-scale (SGS) turbulence model for dynamic

processes but exclude it for cloud microphysics processes, such as collision-coalescence enhancement, velocity fluctuations, and supersaturation fluctuations. This approach might lead to an underestimation of the collision rate of charged droplets, as noted by Lu and Shaw (2015). Our simulations use two-dimensional Large Eddy Simulation (LES) methodology. To assess the impact of fluctuations, we
320 conduct a 50-member ensemble of simulations, varying the pseudo-random number sequence for each run.

2.6 Design of our numerical experiment

To evaluate the effect of electro-coalescence on warm clouds, 2D simulation of an isolated cumulus is
325 performed following the setup of Lasher-Trapp et al. (2005). Note the original study of Lasher-Trapp et al. (2005) was conducted in 3D, but 2D simulation is used in this study to save computational resources. The initial profile of the atmosphere is horizontally uniform. The vertical profile of the moist air is given by 1545 UTC 22 July sounding data from the Small Cumulus Microphysics Study (SCMS) in Florida. The cloud base is steady at 1050 m, and the maximum cloud top height is 5350 m. As suggested by
330 Lasher-Trapp et al. (2005), wind shear is assumed to be absent, and random velocity perturbation is applied (maximum of 0.5 m s^{-1}) in the lowest kilometre of the model.

In general, there are different types of soluble/insoluble aerosols in a droplet. In the model, only one soluble substance ((NH_4) HSO_4 aerosol) is applied for simplicity. Initially, the aerosols are uniformly distributed in the simulation domain. The aerosol number concentration and size distribution were based
335 on the data provided by Van Zanten et al. (2011) for the RICO intercomparison case. The aerosol number concentration and size distribution is given by a bimodal log-normal distribution: The particle number concentrations of the two modes are $N_1 = 90 \text{ cm}^{-3}$ and $N_2 = 15 \text{ cm}^{-3}$, respectively. Note that aerosol concentrations are multiplied by factors of 3, 6, or 9, depending on the aerosol background conditions. The geometric mean radii are $r_1 = 0.03 \text{ }\mu\text{m}$ and $r_2 = 0.14 \text{ }\mu\text{m}$, with geometric standard deviations of
340 $\sigma_1 = 1.28$ and $\sigma_2 = 1.75$, respectively.

3. Results

3.1 The effect of charged droplets on cloud evolution

Figure 2 presents snapshots of cloud structures at 1500 second, 2100 second, and 2700 second from a
345 single simulation, illustrating the temporal changes in the mixing ratios of cloud water and rainwater. The results show that with electro-coalescence by the CS setting (Figs. 2(d)-(i)), the cumulus takes a shorter time to form rain droplets than with that by the CB and no charge (NC) settings. Comparing Figs. 2(d)-(f) and Figs. 2(g)-(i) shows that the electric force with the CS setting has a much stronger impact on the cloud evolution than that with the CB setting. For the CS setting, there is heavy precipitation at 2700
350 second, while there is only haze for the CB and NC settings.

Figure 3(a) shows the time evolution of the domain and 50 ensembles averaged accumulated precipitation amount. Figure 3(b)-(d) shows the domain-averaged pathway, including the total liquid water pathway (b), rainwater pathway (c), and cloud water pathway (d). The error bar indicate the standard error, which is also calculated from the 50 members of the ensemble. An unbiased estimator is used to calculate the standard deviation error. The results show that the accumulated precipitation amount in the CS setting is 52.5 % higher than that in NC setting, 34.9 % higher than CB setting, and 8.4 % higher than IM setting. There is significant difference between the accumulated precipitation amounts in NC setting, CS setting, IM setting and CB setting. The initial precipitation time for four settings all start at 2100 second. However, the total liquid water path and cloud path of the CB and NC settings are significantly higher than those of the CS setting because higher precipitation eliminates cloud evolution.

Figure 4 presents the droplet mass density distributions during three stages of cloud development for the NC, CB, IM, and CS settings. At these three stages, the droplet size distribution in the CS setting is much wider and rain droplets are much coarser than in the NC, IM and CB settings. At 2100 second, there are two mass density peaks of 10 μm and 1000 μm droplets for the NC, IM, CS, and CB settings, while the CS setting shows the highest mass density at 1000 μm , which is consistent with the results of Fig. 3.

3.2 The effect of charge on droplets

Figure 5 shows the results of droplet time evolution (a)-(c) and the water fraction path (d)-(f) for charging rate (α) is 0.1, 0.2, and 0.6; the black line represents the NC setting. The results show that there are no significant differences between the results of the NC and CS settings with the charging rate $\alpha=0.1$, which gives 0.3 % of the maximum charge on the droplets. With the enhancement of the charge on the droplets, clouds can form more rapidly. When the charging rate $\alpha=0.6$, at 1500 second, there are larger droplets with radius over 1000 μm and even droplets sized 5000 μm . However, cloud elimination is faster in higher charging rate condition, at 2700 second, a lower charging rate condition results in a higher droplet mass density at a peak of approximately 1000 μm , which indicates that a higher charging rate results in a shorter lifetime of the cumulus cloud. The results of the domain water path, averaged over 50 ensembles in Figs. 5(d)-(f) are consistent with those in Figs. 5(a)-(c).

Figure 6 shows the domain and 50 ensembles averaged precipitation amount as a function of the droplets charging rate in the CS setting. Similar to the results in Fig. 5, clouds with higher charging rate condition produce precipitation earlier than those under low charging rate conditions. With the enhancement of the charging rate, the precipitation amount at 3500 second does not simultaneously increase under all conditions. When the charging rate is 0.6, the final precipitation amount decreases due to more liquid and cloud water loss in the early stage of cloud formation. In Fig. 6, the result of the CS setting charging rate α equal to 0.05, which is 0.16 % of the maximum charge on the droplets, is given by the solid orange line, which the precipitation amount is 9.5 % higher than that of the NC setting.

3.3 The effect of the aerosol concentration

Figure 7 illustrates the average precipitation amounts for 50 ensemble simulations under the CS setting, plotted as a function of aerosol concentrations. The results are shown for low (solid line), medium (dotted line), and high (dash-dotted line) aerosol concentrations, with a charging rate of 0.2. The blue, pink,

purple lines represent the results of LA, MA and HA conditions with the NC setting. Under NC settings,
390 the Twomey effect demonstrates that higher aerosol concentrations lead to smaller particle radii in clouds,
reducing precipitation efficiency. Conversely, when electrostatic forces are introduced, these higher
aerosol concentrations substantially enhance precipitation across different scenarios. Specifically, in high
aerosol (HA) conditions, the precipitation enhancement reaches 782 % over the NC setting; for medium
aerosol (MA) conditions, it's 467 % higher; and for low aerosol (LA) conditions, the increase is 110 %.
395 This illustrates the significant role electrostatic forces play in modulating cloud dynamics and
precipitation responses to aerosol variations.

3.4 Comparison of different electrostatic force calculations

Figure 8 presents the domain-averaged precipitation amounts under different electrostatic force settings
with a charging rate of 0.3, illustrated by various line styles for each setting. The blue dashed line
400 represents the result of droplets with opposite sign charges and the setting based on Khain04 method.
The upper limit of the charge on the small droplets is 50 elemental charges, the lower limit of the limit
of the charge on the droplets is 1 elemental charge and the pink dashed-dotted line represents the special
setting of only a large droplet charged with electrostatic force by the CS method (CS-q0). For the CS,
Khain04 and IM setting, precipitation increases at 2100 second, which is 300 second before the NC
405 setting. The domain and ensembles averaged precipitation amount with the CS setting is 52.5 % higher
than that with the NC setting; with the Khain04 setting, it is 5.42 % larger; with the CS-q0 setting, it is
9.6 % larger; and with the IM setting, it is 8.45 % larger.

4. Discussion

When the two droplets move together and coalesce, there are three sites where collisions can occur, the
410 front, side and rear. The radius ratio between a large droplet and a small droplet (RARA) controls the
collision site, and when the radius of the small droplet is less than $0.1 \mu\text{m}$ and the RARA is larger than
100, the collision is a rear collision. For front and side collisions, in clouds where the droplet size is less
than $40 \mu\text{m}$ and the relative humidity is 100 %, the droplet collision is controlled by the balance of the
Stokes drag of the air flow and electric force. The analytic expression in our work suggested by
415 Davenport and Peters (1978) can give a good estimation, especially for the Greenfield gap part, although
in the front and side collision regions when the RARA is close to 1, the additional contribution due to
the interception associated with the electric effect cannot be fully reproduced by this method. For the rear
collision, the flow drag, electric force and Brownian motion of the small droplet can impact the collision
process. In the present work, because the charge on the droplet varies as a function of the droplet radius,
420 there is less than 1 elemental charge on a droplet with a radius less than $0.1 \mu\text{m}$. Therefore, the electric
force does not have a significant effect on the collision process even for droplets of opposite signs, and
the Brownian collision efficiency could be good enough for estimation under these conditions. When the
amount of charge on a small droplet is over several elemental charges due to the evaporation of a large
droplet with a large amount of charge, the rear collision could be significantly affected by the electric
425 force (Tinsley and Leddon, 2013). The net attractive force of droplets with opposite signs increases the

collision efficiency, and the net repulsive force of droplets with the same sign decreases the collision efficiency; this is called electro-anti-coalescence. As Tinsley (2001) mentioned, below the cloud bottom boundary, there could be a highly charged nucleus or small droplet with tens to hundreds of elemental charges due to the evaporation of a highly charged droplet. These highly charged small droplets or nuclei
430 could be moved into the cloud by upward air flow, which is not considered in this paper.

In clouds, there are several ways to charge droplets, and in the cloud boundary, due to charging by the vertical electric current density (J_z) from the ionosphere to the ground surface, a droplet in the cloud top boundary accumulates a positive charge, and that in the cloud bottom boundary accumulates a net negative charge; this has been shown by simulations (Zhou and Tinsley, 2007, 2012) and field
435 observations (Nicoll et al., 2016). With the charging rate of 0.05, there are on the order of 100 elemental charges on a droplet with a radius of 10 μm , which is consistent with observation (Beard et al., 2004) and simulation (Zhou and Tinsley, 2007) results. Therefore, in the stratus cloud, most droplet collisions occur between droplets of the same sign or between one charged droplet and one uncharged droplet. Using the CS method, the additional electrostatic force due to the multiple image dipoles between the colliding
440 droplets can be addressed, even if the droplets have the same sign charges or a small droplet is uncharged. Khain et al. (2004) evaluated the electro-coalescence effect on warm clouds rain enhancement and fog formation based on the image charge method from one induced dipole on each droplet by bin scheme. Zhou et al. (2009) claimed that when the RARA is close to 1, the collision efficiency calculated by the CS method, which treats the multiple induced dipoles on each droplet, is twice as large as those calculated
445 with the IM method. Therefore, for the Greenfield gap region and interception region, the evaluation of the charge effect with the CS method is more accurate. And the particle-based approach SDM provide superior performance than bin schemes (Li et al., 2017). In Fig. 8, due to the additional induced image charge on droplets, the maximum averaged precipitation amount of the CS setting is 8.45 % larger than that of the IM setting. Despite a 30 % increase in computation burden, the CS method for electrostatic
450 force should be incorporated into the cloud microphysics scheme. CS method provides superior numerical stability and accuracy in simulating charge droplet interactions, particularly for charge droplets of similar size. Khain et al. (2004) evaluated electro-coalescence at a low charging rate of 5 % of the maximum charge on droplets. In our simulation, we tested charging rates (α) ranging from 0.05 to 0.6, equivalent to 0.15 % to 1.8 % of the maximum charge. At a charging rate of 0.3, the electric force
455 evaluated by the CS method increased domain and ensemble-averaged precipitation by approximately 5.42 % compared to the Khain04 setting. The results indicate that even with weak charging, the electro-coalescence effect significantly increases precipitation.

Tinsley et al. (2001, 2006) and Zhou et al. (2009) claimed that the induced charge on droplets of the same sign could produce a short-range attractive electrostatic force that increases the collision efficiencies.
460 The charge on the large droplets could exert an additional short-range attraction on the small droplet, even if there is no charge or the same charge on the small droplets. However, for droplets of the same sign, the short-range electrostatic force has a significant effect only if the charge ratio between the large droplet and small droplet $Q:q$ is greater than 100 or $q:Q$ is greater than 1. For $Q:q$ ratios larger than 100, the additional image charge effect on the small droplet due to the large charged droplet controls the

465 collision process. For $q:Q$ greater than 1, the additional image charge effect is due to the small charged droplet.

The particle-based approach SDM provides explicitly cloud-aerosol interaction simulation, such as the role of CCN in rain formation (Grabowski et al., 2019). According to our simulation results, the electro-coalescence effect on precipitation is sensitive to the aerosol concentration. With a high aerosol concentration, the average precipitation with an electric effect could be a factor of 4 higher than that of the NC condition. A much higher aerosol concentration corresponds to a more sensitive cloud response to the electrostatic force. Then, under high aerosol concentration conditions, a small variation in J_z could have a significant effect on cloud formation. Alternatively, in highly polluted clouds, placing a small number of charged aerosols or droplets accelerates rain enhancement due to electro-coalescence.

475

5 Conclusion

The electro-coalescence effect on a weakly electrified warm cumulus cloud was revisited. Assuming droplets with opposite signs are charged instantaneously by J_z , the amount of charge is determined by the size of the droplets. A new simulation with the exact treatment of the electrostatic force for opposite sign charge case based on the particle-based approach SDM provides a good estimation of the effect of electro-coalescence in the Greenfield gap region. In the simulation, droplets smaller than $0.1 \mu\text{m}$ are controlled by Brownian motion. The results show that for droplets of opposite signs with the same treatment of the electrostatic force, the cloud evolution can be significantly changed as a function of the arbitrarily prescribed charging rate α . The same sign charge droplets case (Tinsley and Zhou, 2015) and charge amount prediction are necessary for accurate simulation. Electro-coalescence has a larger impact on highly polluted warm cumulus cloud.

Cloud radiation feedback is one of the sources of uncertainty in the climate model (Zelinka et al., 2017). The electrostatic force effect parameterization for different cloud types should be indicated to improve climate model accuracy. This study reveals the electrostatic force effect on warm cumulus clouds, contributing to the parameterization of electrostatic microphysical processes.

Code and data availability. The source code of SCALE is available from <https://scale.riken.jp>, note the SDM code is not accessible through this site. The source code of SCALE-SDM 0.2.5-2.3.0 and single simulation data of $\alpha=0.3$ in four settings of NC, CB, IM, and CS are available from <https://zenodo.org/records/11058066>. All the data used for this study can be reproduced by following the instructions included in the above repository. The data are also deposited in local storage at the University of Hyogo, Japan.

Author contributions. All the authors designed the model and numerical experiments. LM and SS developed the model code and RZ performed the simulations. RZ prepared the manuscript with contributions from all co-authors.

Competing interests. The authors declare that they have no conflicts of interest.

505 **Financial support.** This work was funded in part by the Strategic Priority Research Program of CAS (Grant No. XDB 41000000), the National Science Foundation of China (42271027, 41971020), MEXT KAKENHI (grant no. 18H04448), JSPS KAKENHI (grant nos. 26286089, 20H00225, 23H00149), JST [Moonshot R & D][Grant Number JPMJMS2286], China Scholarship Council (202106140113).

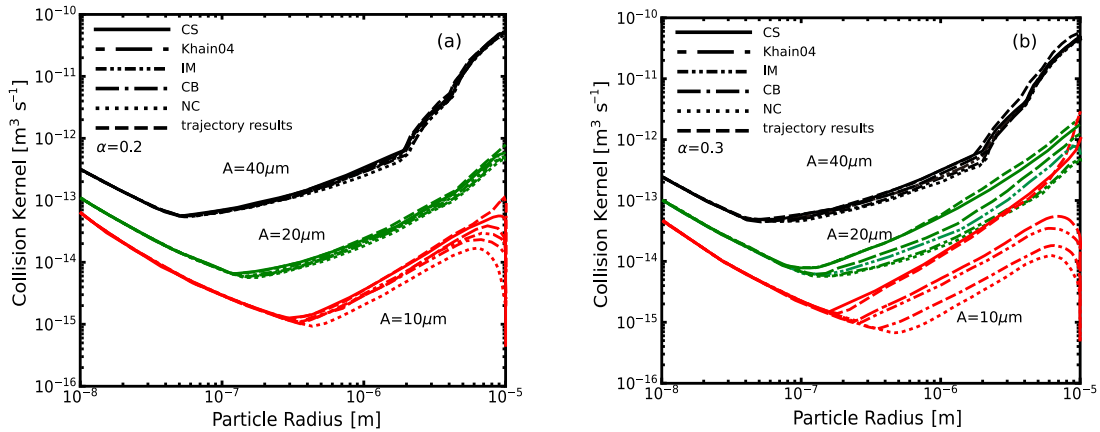
510 **References**

- Andronache, C.: Diffusion and electric charge contributions to below-cloud wet removal of atmospheric ultra-fine aerosol particles, *Journal of Aerosol Science*, 35, 1467-1482, 10.1016/j.jaerosci.2004.07.005, 2004.
- Arabas, S. and Shima, S.-i.: Large-eddy simulations of trade wind cumuli using particle-based microphysics with monte carlo coalescence, *Journal of the Atmospheric Sciences*, 70, 2768-2777, 10.1175/JAS-D-12-0295.1, 2013.
- 515 Arakawa, A. and Lamb, V. R.: Computational design of the basic dynamical processes of the UCLA general circulation model, *Methods in Computational Physics: Advances in Research and Applications*, 173-265, 10.1016/B978-0-12-460817-7.50009-4, 1977.
- 520 Ardon-Dryer, K., Huang, Y. W., and Cziczo, D. J.: Laboratory studies of collection efficiency of sub-micrometer aerosol particles by cloud droplets on a single-droplet basis, *Atmospheric Chemistry and Physics*, 15, 9159-9171, 10.5194/acp-15-9159-2015, 2015.
- Beard, K. V., Ochs III, H. T., and Twohy, C. H.: Aircraft measurements of high average charges on cloud drops in layer clouds, *Geophysical Research Letters*, 31, 10.1029/2004GL020465, 2004.
- 525 Bleaney, B. I., and Bleaney, B.: *Electricity and Magnetism, Volume 1*. Oxford University Press, 676 pp, 1993.
- Bott, A.: A flux method for the numerical solution of the stochastic collection equation, *Journal of the Atmospheric Sciences*, 55, 2284-2293, 10.1175/1520-0469(1998)055<2284:afmftn>2.0.co;2, 1998.
- Craggs., J. M. M. a. J. D.: Electrical breakdown of gases, *Quarterly Journal of the Royal Meteorological Society*, 80, 282-283, 10.1002/qj.49708034425, 1954.
- 530 Davenport, H. M. and Peters, L. K.: Field studies of atmospheric particulate concentration changes during precipitation, *Atmospheric Environment* (1967), 12, 997-1008, 10.1016/0004-6981(78)90344-X, 1978.
- Davis, M. H.: Two charged spherical conductors in a uniform electric field: Forces and field strength, *The Quarterly Journal of Mechanics and Applied Mathematics*, 17, 499-511, 10.1093/qjmam/17.4.499, 1964.
- 535 Davis, M. H.: Collisions of small cloud droplets: gas kinetic effects, *Journal of Atmospheric Sciences*, 29, 911-915, 10.1175/1520-0469(1972)029<0911:COSSCDG>2.0.CO;2, 1972.
- Frederick, J. E. and Tinsley, B. A.: The response of longwave radiation at the South Pole to electrical and magnetic variations: Links to meteorological generators and the solar wind, *Journal of Atmospheric and Solar-Terrestrial Physics*, 179, 214-224, 10.1016/j.jastp.2018.08.003, 2018.
- 540 Frederick, J. E., Tinsley, B. A., and Zhou, L.: Relationships between the solar wind magnetic field and ground-level longwave irradiance at high northern latitudes, *Journal of Atmospheric and Solar-Terrestrial Physics*, 193, 10.1016/j.jastp.2019.105063, 2019.
- Grabowski, W. W., Morrison, H., Shima, S.-I., Abade, G. C., Dziekan, P., and Pawlowska, H.: Modeling of Cloud Microphysics: Can We Do Better?, *Bulletin of the American Meteorological Society*, 100, 655-672, <https://doi.org/10.1175/BAMS-D-18-0005.1>, 2019.
- 545 Greenfield, S. M.: Rain scavenging of radioactive particulate matter from the atmosphere, *Journal of Atmospheric Sciences*, 14, 115-125, 10.1175/1520-0469(1957)014<0115:RSORPM>2.0.CO;2, 1957.

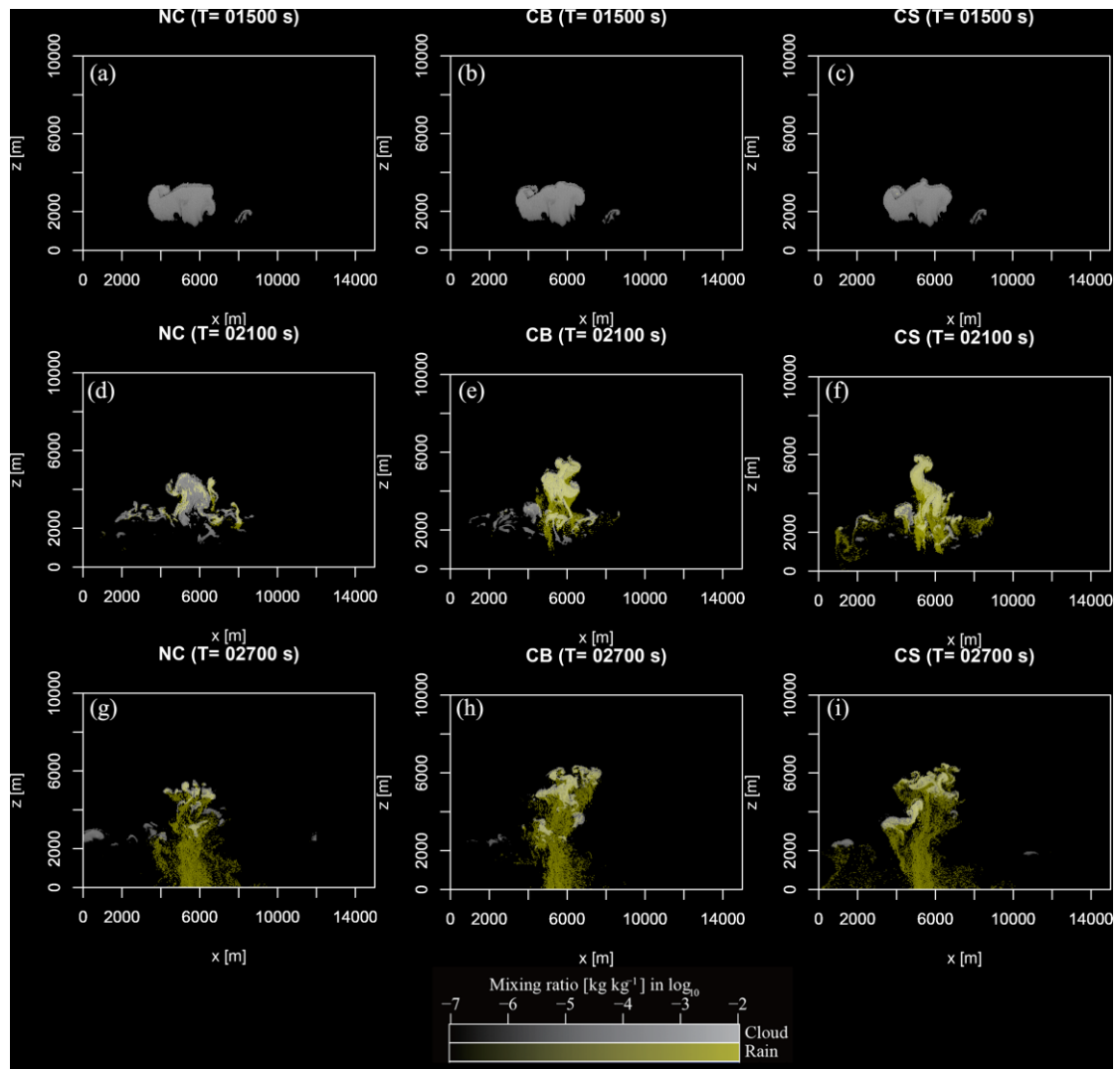
- Hall, W. D.: A detailed microphysical model within a two-dimensional dynamic framework: model
550 description and preliminary results, *Journal of Atmospheric Sciences*, 37, 2486-2507, 10.1175/1520-
0469(1980)037<2486:ADMMWA>2.0.CO;2, 1980.
- Jonas, P. R.: The collision efficiency of small drops, *Quarterly Journal of the Royal Meteorological
Society*, 98, 681-683, 10.1002/qj.49709841717, 1972.
- Khain, A., Arkipov, V., Pinsky, M., Feldman, Y., and Ryabov, Y.: Rain enhancement and fog
555 elimination by seeding with charged droplets. part I: theory and numerical simulations, *Journal of
Applied Meteorology*, 43, 1513-1529, 10.1175/JAM2131.1, 2004.
- Kniveton, D. R., Tinsley, B. A., Burns, G. B., Bering, E. A., and Troshichev, O. A.: Variations in global
cloud cover and the fair-weather vertical electric field, *Journal of Atmospheric and Solar-Terrestrial
Physics*, 70, 1633-1642, 10.1016/j.jastp.2008.07.001, 2008.
- 560 Köhler, H.: The nucleus in and the growth of hygroscopic droplets, *Transactions of the Faraday Society*,
32, 1152-1161, 10.1039/TF9363201152, 1936.
- Fuchs, N. A.: *The Mechanics of Aerosols*, Revised and Enlarged, Pergamon Press Oxford, Oxford, 1964.
- Lam, M. M., Chisham, G., and Freeman, M. P.: Solar wind-driven geopotential height anomalies
originate in the Antarctic lower troposphere, *Geophysical Research Letters*, 41, 6509-6514,
565 10.1002/2014GL061421, 2014.
- Lasher-Trapp, S. G., Cooper, W. A., and Blyth, A. M.: Broadening of droplet size distributions from
entrainment and mixing in a cumulus cloud, *Quarterly Journal of the Royal Meteorological Society*, 131,
195-220, 10.1256/qj.03.199, 2005.
- Li, X.-Y., Brandenburg, A., Haugen, N. E. L., and Svensson, G.: Eulerian and Lagrangian approaches to
570 multidimensional condensation and collection, *Journal of Advances in Modeling Earth Systems*, 9, 1116-
1137, <https://doi.org/10.1002/2017MS000930>, 2017.
- Liu, Y., Yau, M.-K., Shima, S.-i., Lu, C., and Chen, S.: Parameterization and Explicit Modeling of Cloud
Microphysics: Approaches, Challenges, and Future Directions, *Advances in Atmospheric Sciences*, 40,
747-790, 10.1007/s00376-022-2077-3, 2023.
- 575 Lu, J. and Shaw, R. A.: Charged particle dynamics in turbulence: Theory and direct numerical
simulations, *Physics of Fluids*, 27, 10.1063/1.4922645, 2015.
- Meek, J. M. and Craggs, J. D.: Electrical breakdown of gases., *Quarterly Journal of the Royal
Meteorological Society*, 80, 282-283, 10.1002/qj.49708034425, 1954.
- Montero-Martínez, G., Kostinski, A. B., Shaw, R. A., and García-García, F.: Do all raindrops fall at
580 terminal speed?, *Geophysical Research Letters*, 36, <https://doi.org/10.1029/2008GL037111>, 2009.
- Nicoll, K. A. and Harrison, R. G.: Stratiform cloud electrification: comparison of theory with multiple
in-cloud measurements, *Quarterly Journal of the Royal Meteorological Society*, 142, 2679-2691,
10.1002/qj.2858, 2016.
- Nishizawa, S., Yashiro, H., Sato, Y., Miyamoto, Y., and Tomita, H.: Influence of grid aspect ratio on
585 planetary boundary layer turbulence in large-eddy simulations, *Geoscientific Model Development*, 8,
3393-3419, 10.5194/gmd-8-3393-2015, 2015.
- Pruppacher, H. R. and Klett, J. D.: *Microphysics of clouds and precipitation*, Springer Dordrecht,
10.1007/978-0-306-48100-0, 2010.

- Sato, Y., Shima, S.-i., and Tomita, H.: A grid refinement study of trade wind cumuli simulated by a Lagrangian cloud microphysical model: the super-droplet method, *Atmospheric Science Letters*, 18, 359-365, 10.1002/asl.764, 2017.
- Rayleigh, L.: The influence of electricity on colliding water drops, *Proceedings of the Royal Society of London*, 28, 405-409, <https://www.jstor.org/stable/113853>, 1878.
- Rogers, R. R. and Yau, M. K. : A Short Course in Cloud Physics, Elsevier Science, 1989.
- Sato, Y., Nishizawa, S., Yashiro, H., Miyamoto, Y., Kajikawa, Y., and Tomita, H.: Impacts of cloud microphysics on trade wind cumulus: which cloud microphysics processes contribute to the diversity in a large eddy simulation?, *Progress in Earth and Planetary Science*, 2, 23, 10.1186/s40645-015-0053-6, 2015.
- Sato, Y., Shima, S.-i., and Tomita, H.: Numerical convergence of shallow convection cloud field simulations: comparison between double-moment Eulerian and particle-based Lagrangian microphysics coupled to the same dynamical core, *Journal of Advances in Modelling Earth Systems*, 10, 1495-1512, 10.1029/2018MS001285, 2018.
- Seeßelberg, M., Trautmann, T., and Thorn, M.: Stochastic simulations as a benchmark for mathematical methods solving the coalescence equation, *Atmospheric Research*, 40, 33-48, 10.1016/0169-8095(95)00024-0, 1996.
- Seinfeld, J. H. and Pandis, S. N.: *Atmospheric Chemistry and Physics: From Air Pollution to Climate Change*, Wiley, 2006.
- Shima, S.-i., Hasegawa, K., and Kusano, K.: Preliminary numerical study on the cumulus-stratus transition induced by the increase of formation rate of aerosols, *Low Temperature Science*, 72, 249-264, <http://hdl.handle.net/2115/55063>, 2014. (In Japanese)
- Shima, S.-i., Sato, Y., Hashimoto, A., and Misumi, R.: Predicting the morphology of ice particles in deep convection using the super-droplet method: development and evaluation of SCALE-SDM 0.2.5-2.2.0, -2.2.1, and -2.2.2, *Geoscientific Model Development*, 13, 4107-4157, 10.5194/gmd-13-4107-2020, 2020.
- Shima, S., Kusano, K., Kawano, A., Sugiyama, T., and Kawahara, S.: The super-droplet method for the numerical simulation of clouds and precipitation: a particle-based and probabilistic microphysics model coupled with a non-hydrostatic model, *Quarterly Journal of the Royal Meteorological Society*, 135, 1307-1320, 10.1002/qj.441, 2009.
- Tinsley, B. A.: The global atmospheric electric circuit and its effects on cloud microphysics, *Reports on Progress in Physics*, 71, 066801, 10.1088/0034-4885/71/6/066801, 2008.
- Tinsley, B. A. and Leddon, D. B.: Charge modulation of scavenging in clouds: Extension of Monte Carlo simulations and initial parameterization, *Journal of Geophysical Research: Atmospheres*, 118, 8612-8624, 10.1002/jgrd.50618, 2013.
- Tinsley, B. A. and Zhou, L.: Initial results of a global circuit model with variable stratospheric and tropospheric aerosols, *Journal of Geophysical Research*, 111, D16205, 10.1029/2005jd006988, 2006.
- Tinsley, B. A. and Zhou, L.: Parameterization of aerosol scavenging due to atmospheric ionization, *Journal of Geophysical Research: Atmospheres*, 120, 8389-8410, 10.1002/2014jd023016, 2015.

- Tinsley, B. A., Rohrbaugh, R. P., and Hei, M.: Electroscavenging in clouds with broad droplet size distributions and weak electrification, *Atmospheric Research*, 59-60, 115-135, 10.1016/s0169-8095(01)00112-0, 2001.
- 630 Tripathi, S. N., Vishnoi, S., Kumar, S., and Harrison, R. G.: Computationally efficient expressions for the collision efficiency between electrically charged aerosol particles and cloud droplets, *Quarterly Journal of the Royal Meteorological Society*, 132, 1717-1731, <https://doi.org/10.1256/qj.05.125>, 2006.
- Tripathi, S. N., Michael, M., and Harrison, R. G.: Profiles of Ion and Aerosol Interactions in Planetary Atmospheres, *Space Science Reviews*, 137, 193-211, 10.1007/s11214-008-9367-7, 2008.
- 635 Unterstrasser, S., Hoffmann, F., and Lerch, M.: Collection/aggregation algorithms in Lagrangian cloud microphysical models: rigorous evaluation in box model simulations, *Geoscientific Model Development*, 10, 1521-1548, 10.5194/gmd-10-1521-2017, 2017.
- VanZanten, M. C., Stevens, B., Nuijens, L., Siebesma, A. P., Ackerman, A. S., Burnet, F., Cheng, A., Couvreux, F., Jiang, H., Khairoutdinov, M., Kogan, Y., Lewellen, D. C., Mechem, D., Nakamura, K.,
- 640 Noda, A., Shipway, B. J., Slawinska, J., Wang, S., and Wyszogrodzki, A.: Controls on precipitation and cloudiness in simulations of trade-wind cumulus as observed during RICO, *Journal of Advances in Modeling Earth Systems*, 3, M06001, 10.1029/2011MS000056, 2011.
- Wang, F., Zhang, Y., and Zheng, D.: Impact of updraft on neutralized charge rate by lightning in thunderstorms: A simulation case study, *Journal of Meteorological Research*, 29, 997-1010, 10.1007/s13351-015-5023-9, 2015.
- 645 Wang, P. K., Grover, S. N., and Pruppacher, H. R.: On the effect of electric charges on the scavenging of aerosol particles by clouds and small raindrops, *Journal of Atmospheric Sciences*, 35, 1735-1743, 10.1175/1520-0469(1978)035<1735:OTEOEC>2.0.CO;2, 1978.
- Weon, B. M. and Je, J. H.: Charge-induced wetting of aerosols, *Applied Physics Letters*, 96, 194101, 10.1063/1.3430007, 2010.
- 650 Zelinka, M. D., Randall, D. A., Webb, M. J., and Klein, S. A.: Clearing clouds of uncertainty, *Nature Climate Change*, 7, 674-678, 10.1038/nclimate3402, 2017.
- Zhang, L., Tinsley, B. A., and Zhou, L.: Parameterization of in-cloud aerosol scavenging due to atmospheric ionization: Part 3. effects of varying droplet radius, *Journal of Geophysical Research: Atmospheres*, 123, 10546–10567, 10.1029/2018jd028840, 2018.
- 655 Zhou, L. and Tinsley, B. A.: Production of space charge at the boundaries of layer clouds, *Journal of Geophysical Research: Atmospheres*, 112, D11203, 10.1029/2006jd007998, 2007.
- Zhou, L. and Tinsley, B. A.: Time dependent charging of layer clouds in the global electric circuit, *Advances in Space Research*, 50, 828-842, 10.1016/j.asr.2011.12.018, 2012.
- 660 Zhou, L., Tinsley, B. A., and Plemmons, A.: Scavenging in weakly electrified saturated and subsaturated clouds, treating aerosol particles and droplets as conducting spheres, *Journal of Geophysical Research*, 114, D18201, 10.1029/2008jd011527, 2009.



670 **Figure 1: Comparison of the effect of electric charge on the collision kernel for droplets sized $40 \mu\text{m}$, $20 \mu\text{m}$**
and $10 \mu\text{m}$ with small droplet radii between $10^{-2} \mu\text{m}$ and $10 \mu\text{m}$. The charging rate α is 0.2 for panel (a) and
0.3 for panel (b). The solid line represents the results where the collision kernel is calculated by the analytical
expression and treats the charged droplets as CS setting. The long-dashed line represents the results
calculated by the analytical expression and treats the charge droplets as Khain04 setting. The dashed-dotted-
675 dashed-dotted line represents the results calculated by the analytical expression and treats the electrostatic electric
force by the IM setting. The dashed-dotted line represents the results calculated by the analytical expression
and treats the electrostatic electric force by the CB setting. The dotted line shows the results with NC setting.
The dashed line represents the results of the trajectory simulation according to Zhou et al. (2009).



680

Figure 2: A comparison of the spatial structure of the mixing ratio of hydrometeors of the cumulus with NC setting, the electric force evaluated by CB setting and the electrostatic electric force evaluated by CS setting at times of 1500 s, 2100 s and 2700 s. The charging rate α is 0.3.

685

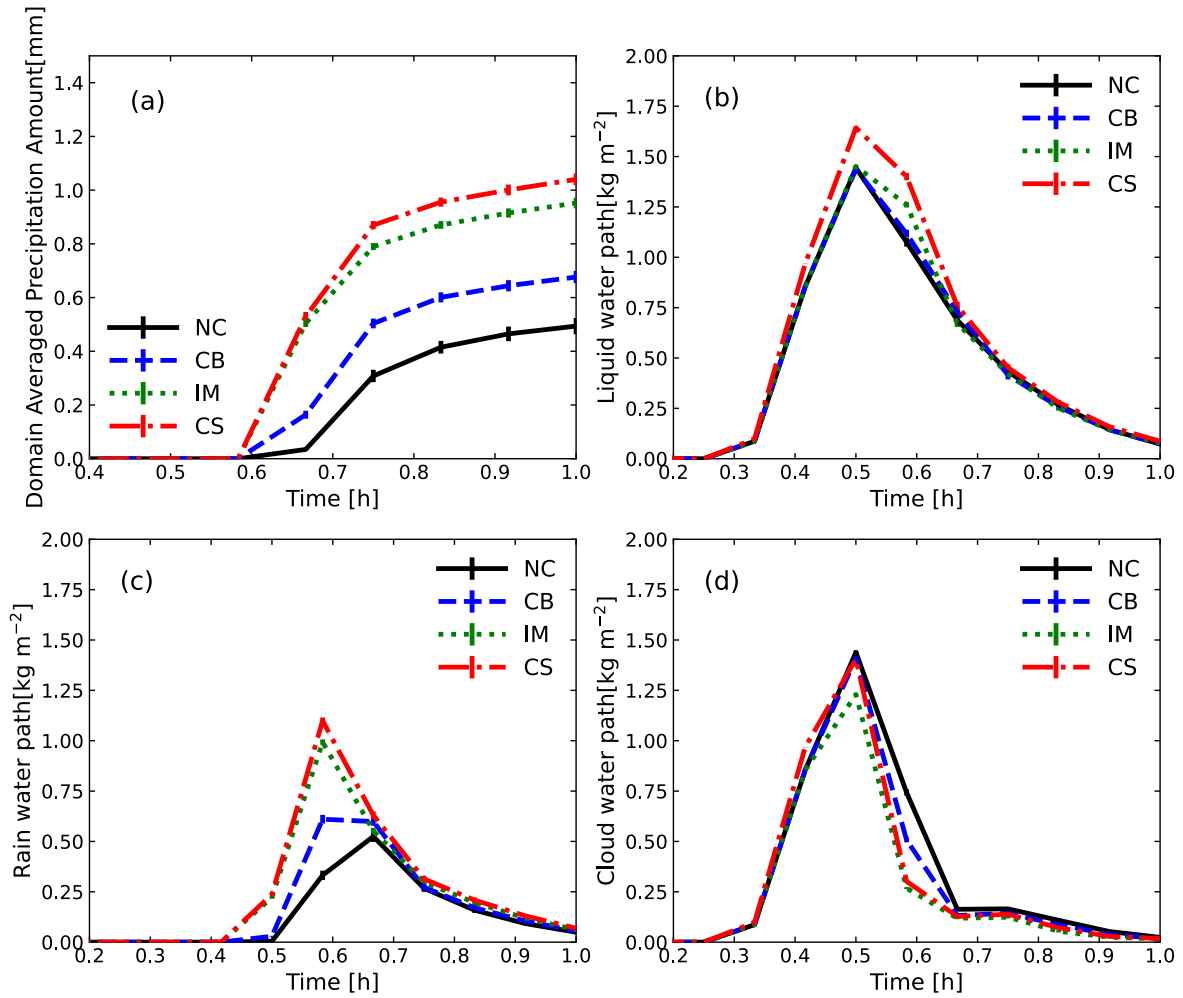
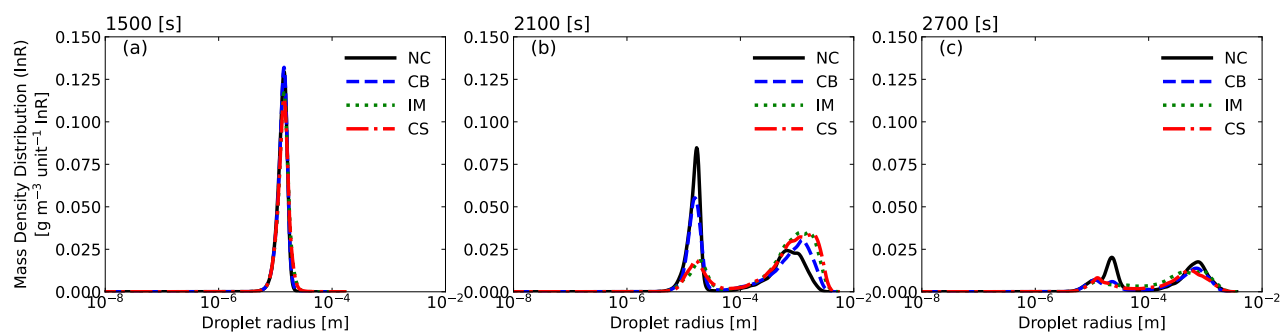


Figure 3: The time evolution of the domain-averaged precipitation amount (a) and the domain-averaged water path of the liquid water path (b), rainwater path (c) and cloud water path (d), which is consistent with Fig. 2. The black solid line represents NC setting, the blue dashed line represents CB setting, the green dot line represents IM setting, and the red dashed-dotted line represents CS setting. The error bar indicates the standard deviation calculated from 50 members of the random ensemble.

690

695

700



705 **Figure 4:** The mass density distribution evolution of the droplets at 1500 s (a), 2100 s (b) and 2700 s (c), which is consistent with Fig. 2 and Fig. 3. The black solid line represents NC setting, the blue dashed line represents CB setting, the green dotted line represents IM settings and the red dashed-dotted line represents CS setting.

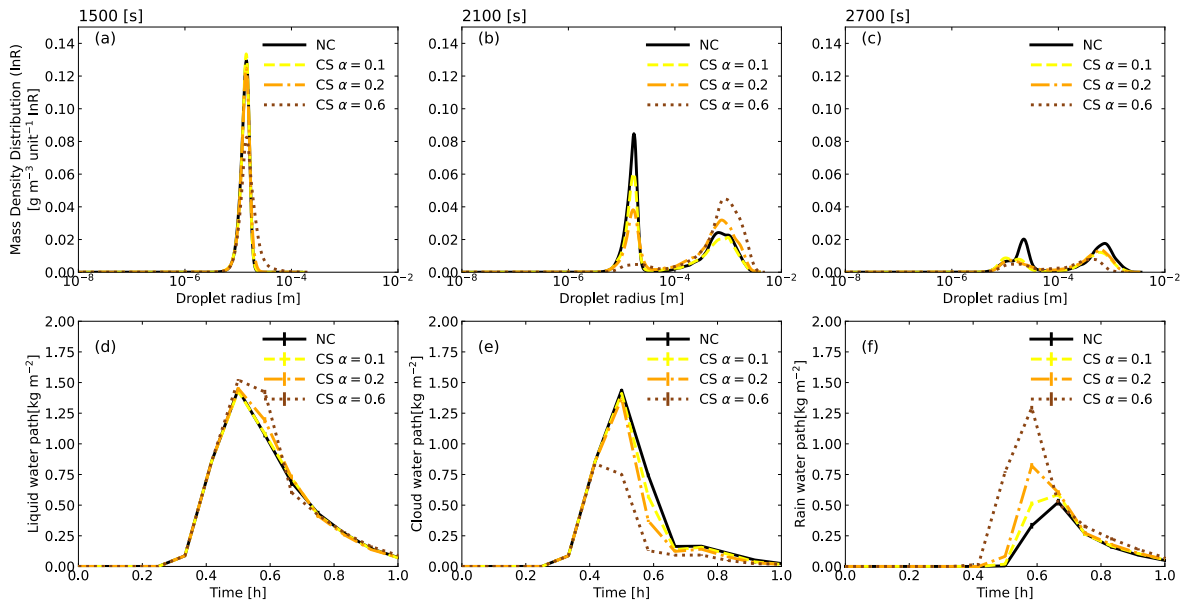
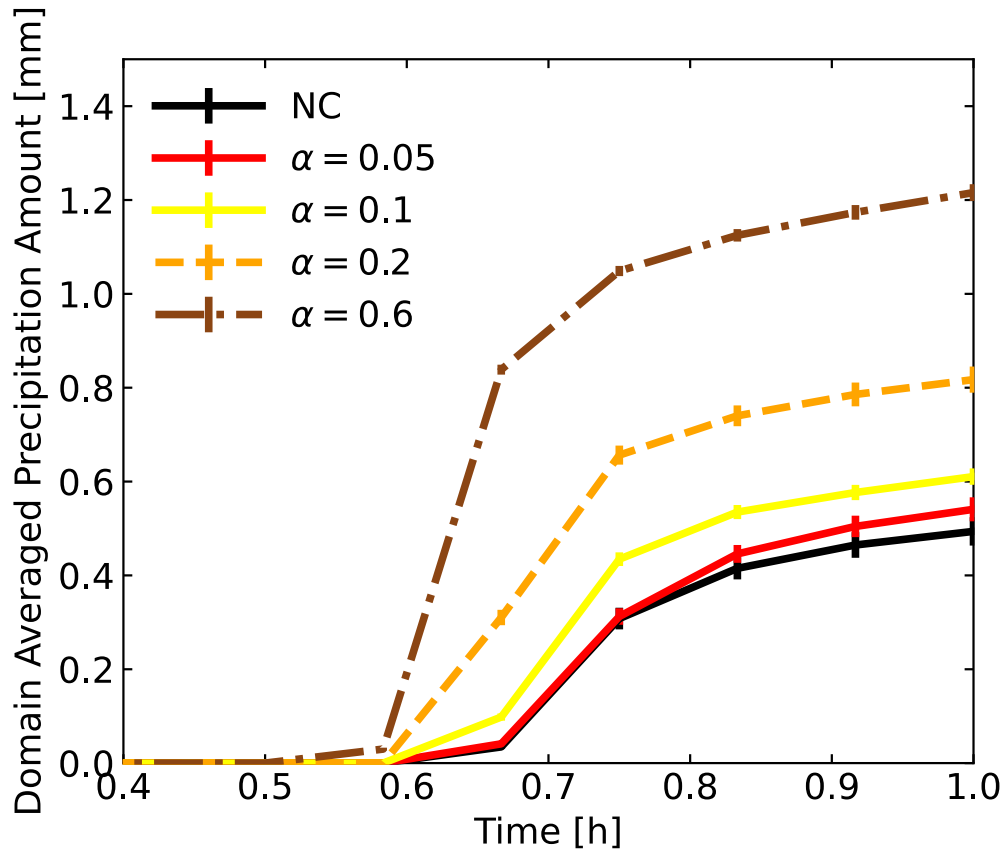
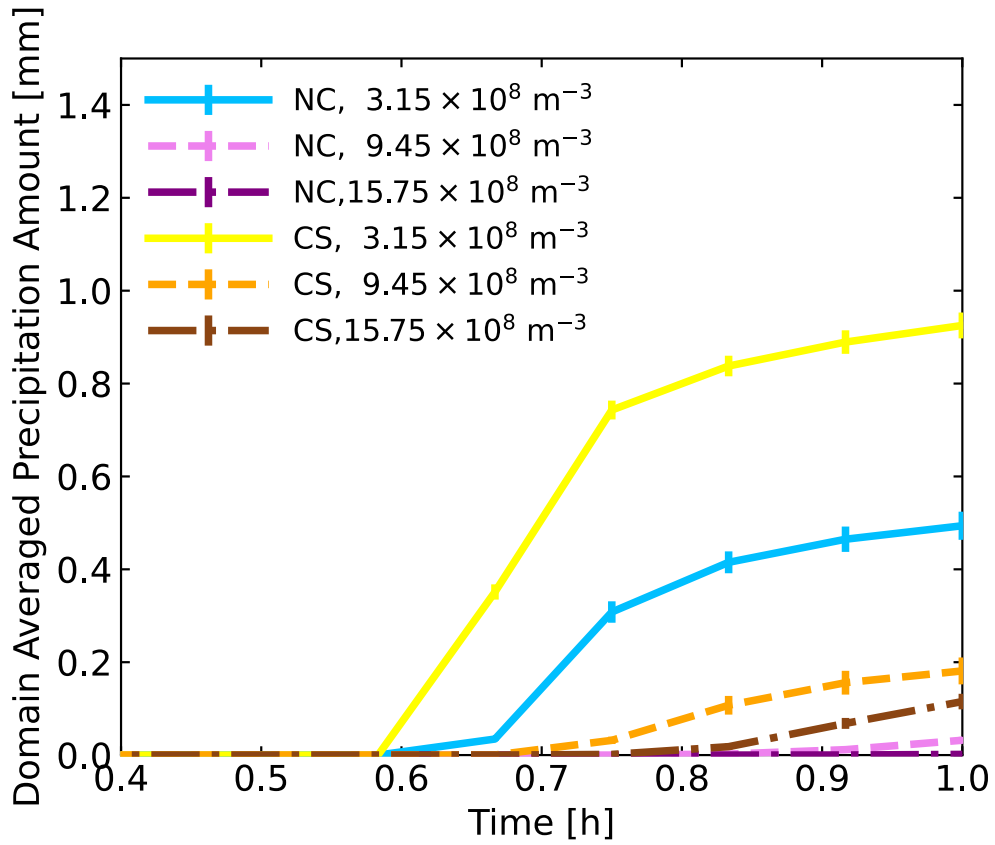


Figure 5: Comparison of the cloud evolution for variable charging rates. The mass density distribution of droplets at 1500s (a), 2100s (b) and 2700s (c) and time evolution of the domain-averaged water path of liquid water path (LWP) (d), cloud water path (CWP) (e), and rain water path (RWP) (f) are presented for charging rate α is 0.1 (yellow solid line), 0.2 (orange dashed-dotted line) and 0.6 (brown dotted line).



720 Figure 6: A comparison of the evolution of the domain-averaged precipitation amount with variable droplet charging rate α is 0.05 (red solid line), 0.1 (yellow solid line), 0.2 (orange dashed line), and 0.6 (brown dashed-dotted line), and the electric force is evaluated with the CS setting. The black solid line represents the NC setting.

725

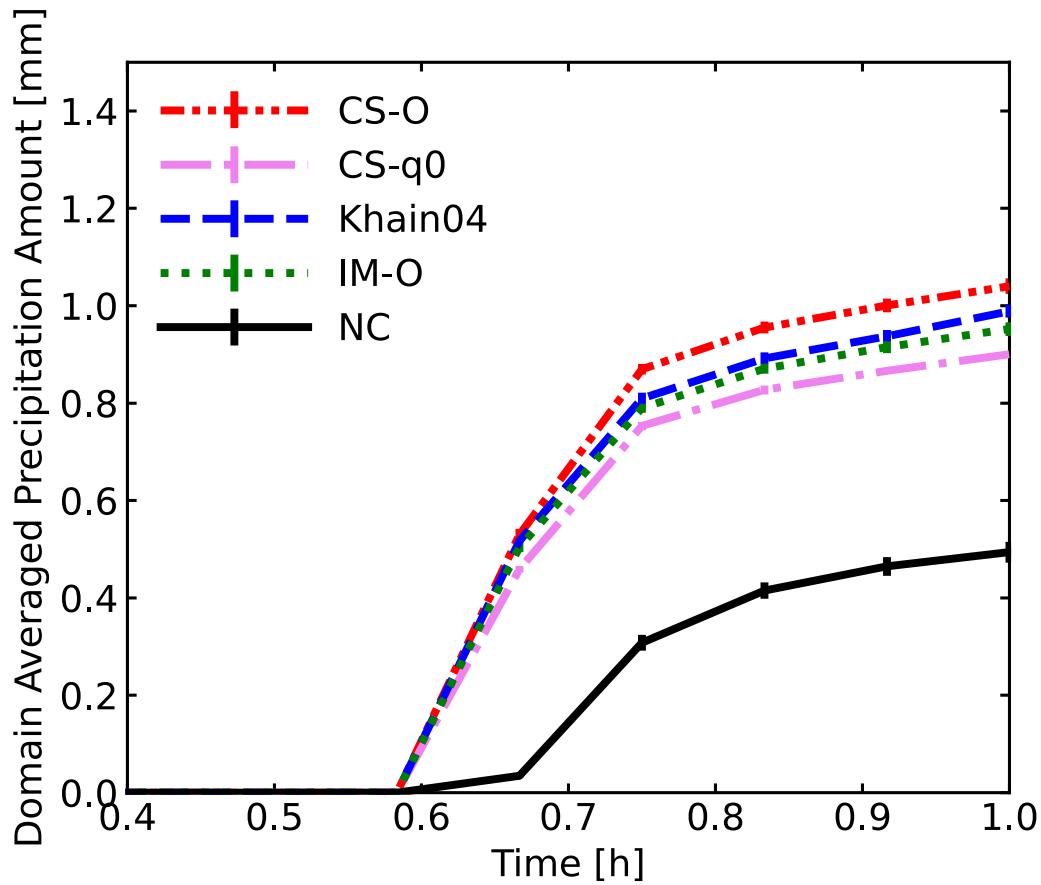


730

Figure 7: The time evolution of the domain-averaged precipitation of the aerosol concentration represented by solid lines (LA, $3.15 \times 10^8 / \text{m}^3$), dotted lines (MA, $9.45 \times 10^8 / \text{m}^3$) and dashed-dotted lines (HA, $15.75 \times 10^8 / \text{m}^3$). The yellow, orange, brown lines represent the simulation with the electric force in LA, MA, HA respectively, which is evaluated with the CS setting, the charging rate α is 0.2. And blue, pink, purple lines represent the simulation with NC setting in LA, MA, HA respectively.

735

740



745 Figure 8: Comparison of the time evolution of the domain-averaged precipitation amount for variable
 750 evaluation of the electric force. The black solid line represents the NC setting. The dashed-dotted lines
 represent the results of the electric force evaluated by the CS method. The red dashed-dotted line represents
 the result of droplets of with opposite sign charges. The pink dashed-dotted line represents the condition
 where the charge is only on the large droplet, the blue dashed line represents the result of droplets with
 opposite sign charges and the CS method based on Khain et al. (2004). The green dotted line is the result of
 droplets with opposite sign charges, and the electric force is evaluated by the image charge method.